
Title: Microcellular polymer films based on cross-linked 1-vinyl-2-pyrrolidone and methyl methacrylate

Authors: José A. Reglero Ruiz, Saúl Vallejos, Blanca S. Pascual, Cipriano Ramos, Sagrario Beltrán, Félix C. García, José M. García

PII: S0896-8446(18)30318-8
DOI: https://doi.org/10.1016/j.supflu.2018.07.011
Reference: SUPFLU 4325

To appear in: *J. of Supercritical Fluids*

Received date: 15-5-2018
Revised date: 9-7-2018
Accepted date: 9-7-2018

Please cite this article as: Ruiz JAR, Vallejos S, Pascual BS, Ramos C, Beltrán S, García FC, García JM, Microcellular polymer films based on cross-linked 1-vinyl-2-pyrrolidone and methyl methacrylate, *The Journal of Supercritical Fluids* (2018), https://doi.org/10.1016/j.supflu.2018.07.011

# Microcellular polymer films based on cross-linked 1-vinyl-2-pyrrolidone and methyl methacrylate

José A. Reglero Ruiz[1,*], Saúl Vallejos[1], Blanca S. Pascual[1], Cipriano Ramos[2], Sagrario Beltrán[2], Félix C. García[1] and José M. García[1]

[1] Departamento de Química, Facultad de Ciencias, Universidad de Burgos, Plaza de Misael Bañuelos s/n, 09001 Burgos, Spain. Tel: +34 947 258 085; Fax: +34 947 258 831.

[2] Departamento de Biotecnología y Ciencia de los Alimentos, Facultad de Ciencias, Universidad de Burgos, Plaza de Misael Bañuelos s/n, 09001 Burgos, Spain. Tel: +34 947 258 085; Fax: +34 947 258 831.

* Corresponding author email: jareglero@ubu.es

Graphical abstract

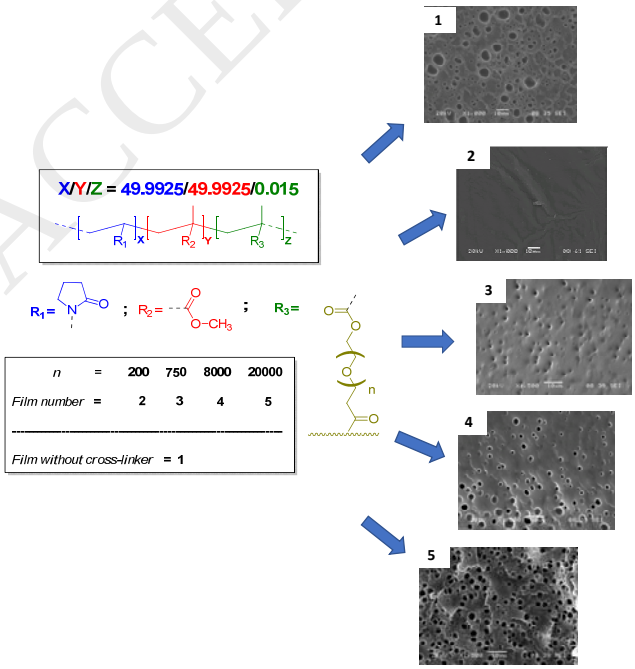

## Highlights

- Crosslinked microcellular polymeric films were foamed using $ScCO_2$.
- Cellular structure was controlled through the molecular mass of the cross-linker.
- The mechanical properties of films were determined by low-velocity tensile tests.
- Young's modulus of the films and the crosslinker molecular mass were correlated.

## Abstract

A series of cross-linked copolymer films based on 1-vinyl-2-pyrrolidone and methyl methacrylate were produced using different poly(ethylene glycol) dimethacrylates as cross-linking agents. The average molecular mass of the cross-linking agent was varied, then allowing the foaming process using supercritical $CO_2$ ($ScCO_2$), obtaining microcellular films with different cellular structures as a function of the molecular mass of the cross-linking agent. The chemical structure, swelling behavior, $CO_2$ uptake and cellular morphology of the materials were studied. Finally, the influence of the different cross-linking agents in the mechanical properties was also evaluated by measuring the tensile properties of the microcellular films.

Keywords: microcellular polymer foam; films; cross-linking; tensile properties; $ScCO_2$ foaming

## 1 – Introduction

In the last two decades, supercritical carbon dioxide ($ScCO_2$) has been used as foaming agent to obtain microcellular polymer foams. $CO_2$ presents numerous advantages, such as: non-toxicity, inertness, non-expensive and it can be easily employed in supercritical state in several processing applications due to the accessible critical conditions (31 ºC and 73 bar).

Concerning polymer foaming, $CO_2$ presents a good solubility in amorphous polymers, and it is employed in dissolution gas foaming processes to obtain micro and nanocellular polymers [1]. The foaming process begins with the saturation of the polymer with $CO_2$ in the supercritical regime, during a fixed time. After saturation of the sample, approaching or being in a rubbery state, system is depressurized to atmospheric pressure, taking advantage of the swelling and plasticization of the polymer, reducing the glass transition temperature, allowing the gas expansion. The cellular microstructure may be controlled by changing the saturation temperature and the depressurization rates. In the last years, the improvement of the processing techniques have led to the obtention of nanoporous polymeric materials, in which new properties have emerged due to the reduction of the cell size (i.e., below 200 nm) [2]. One of the most promising and analyzed properties is the thermal conductivity, which decreases drastically when reducing the cell size, due to the apparition of the knudsen effect [3], thus obtaining low-density polymers with super-isolating properties [4]. In this investigation line, our group has recently published a research work focused on the thermal properties of microcellular polymer foams based on 1-vinyl-2-pyrrolidone and butyl acrylate [5]. The physical properties of nanocellular polymers has been reviewed by Notario *et al.* [6].

In parallel, there is an increasing interest in the development of porous polymer thin films, due to the important number of applications based on these materials. The classical techniques include the use of organic solvent in several steps reactions. However, the use of $ScCO_2$ to generate nanoporous polymer films has attracted great attention only in the last years [7]. In this sense,

different research works have been published reporting the fabrication of different micro or nano cellular polymeric films using $ScCO_2$ as foaming agent [8-9], but there are still several difficulties to overcome, mainly related to the rapid diffusion of the $CO_2$ out of the polymer during the depressurization process. The research works presented by Siripurapu *et al.* analyze the use of different processing parameters and inorganic charges to produce microcellular polymeric films based on PMMA [10-11], but only a few promising results have been reported up to date.

The confinement of the $CO_2$ during the depressurization process is one of the key problems to obtain homogeneous micro and nanocellular polymeric films. In this sense, the use of different chemical cross-linking agents, added to the polymer matrix, can retain the $CO_2$ molecules during the depressurization process, thus controlling the cellular structure parameters (cell density and cell size), as a function of the cross-linking agent employed [12-13]. In our case, the use of methacrylate-based crosslinking agents is particularly interesting due to their good $CO_2$-philicity, thus enhancing their foamability behavior [14]. Another interesting alternative is the use of physical cross-linking process, in which the polymer is irradiated with electrons to difficult the molecular movement, stabilizing the structure during the foaming process. This research line focuses the last published works of different authors, analyzing both the physical foaming using $ScCO_2$ and also the use of chemical blowing agents [15-17]. On the contrary, it is well know that the use of cross-linking agents in $ScCO_2$ foaming can difficult the $CO_2$ sorption process, thus limiting the nucleation sites and the formation of the cellular structure.

The study of mechanical properties of foamed polymers is also a very interesting topic, especially when cell size is reduced down to micro and nanocellular range. In this sense, microcellular polymer foams offer improved toughness, strength, and stiffness respect to solid polymers. , thermal insulation in nanocellular materials has been extensively analyzed during decades, but on the other hand, the research associated to the mechanical properties of these

materials has only increased recently. Following this investigation line, different authors have presented several works in the last years focused in the analysis of different mechanical properties (compression, tensile or impact), of micro and nanocellular amorphous polymers (mainly PMMA and PEI) obtained using $ScCO_2$ [18-21].

Bearing all these ideas in mind, in this work we present a procedure to obtain microcellular amorphous polymeric films using $ScCO_2$ as foaming agent with controlled morphological structure through the addition of a crosslinker agent with different molecular masses. Film is placed between two steel plates during the saturation process, then confining the $CO_2$ during the depressurization process, allowing the formation of the microcellular structure [9,10]. The addition of different cross-linking agents, based on poly(ethylene glycol) dimethacrylates with different molecular masses (between 200 and 20000), tunes the cellular structure, in terms of homogeneity and cell size, and also the mechanical properties. To evaluate and quantify this correlation, the Young's modulus, elongation at break and tensile strength of the microcellular films were analyzed through low-velocity tensile tests.

## 2 - Experimental

### *2.1 – Materials*

All materials were used as received and were commercially available. The list includes: 1-vinyl-2-pyrrolidone (**VP**) (Aldrich, >99%), methyl-methacrylate (**MMA**) (Aldrich, >99%), and poly(ethylene glycol) dimethacrylate as cross-linking agent (**PEGDMA**) with different molecular masses (200, 750, 8000 and 20000). **$PEGDMA_{200}$**, **$PEGDMA_{750}$** and **$PEGDMA_{20000}$** were supplied by Aldrich, (>98%), whereas **$PEGDMA_{8000}$** was supplied by Alfa Aesar (>98%). 2,2-dimethoxy-2-phenylacetophenone was used as UV photo-initiator (**Fotoi**) (Aldrich >99%).

*2.2 – Film preparation*

Films were prepared via a simple bulk radical copolymerization process, which is extensively described in detail in one of our previous works [21]. **VP** was copolymerized with **MMA** and the corresponding **PEGDMA**, with proportions 49.9925/49.9925/0.015 (molar feed ratio), using **Fotoi** (0.16 wt.%) as UV radical photo-initiator. As a consequence, we maintained the nominal cross-linking ratio (*X*) value fixed to $3 \cdot 10^{-4}$ mol **PEGDMA**/mol **VP** and also to $3 \cdot 10^{-4}$ mol **PEGDMA**/mol **MMA** (value of *X* can be easily calculated as the percentage of the ratio between the moles of the cross-linker and the moles of each monomer). Then, the cross-linking density was kept constant to eliminate the influence of this parameter in the foaming behavior. Bulk radical polymerization reaction was carried out in a silanized glass mold (100 μm thick) in an oxygen-free atmosphere at RT overnight. The chemical structure of the films is presented in Scheme 1. The films were transparent, flexible and also easily manageable.

**Scheme 1**.

*2.3 – Foaming experiments*

Foaming took place in a single-step batch process using $ScCO_2$. Films were cut in pieces of 35x35 $mm^2$, and sandwiched between 2 steel plates of 2 mm thickness, to confine the gas during depressurization, thus limiting the gas diffusion process outside the material. Samples were saturated in a high-pressure reactor of 2 L capacity at 35 MPa and 60 °C during 8 h. Depressurization was carried out using a manual opening valve, with a depressurization time about 10 s. Three different samples of each material were foamed in each batch. It is important to remark that preliminary foaming tests were performed to determine the optimum foaming conditions for this particular blend. Two different saturation temperatures, 30 and 40 ºC were previously analyzed, keeping 35 MPa as saturation pressure. It was found that sample 1, without cross-linker, was effectively foamed at both temperatures. However, it was necessary to

increase the saturation temperature to 60 ºC to plasticize samples including the cross-linker in their formulation and obtain the foamed films. For this reason, a single batch foaming test at the previous described conditions (35 MPa and 60 ºC) was established for all the samples. Foamed films are listed as 1f, 2f, 3f, 4f and 5f.

*2.4 – Physical characterization*

Characterization of the membranes was carried out using the next instrumental techniques. Infrared spectra (FT-IR) were recorded with a JASCO FT-IR 4200 (4000-400 $cm^{-1}$) spectrometer, equipped with an ATR (Attenuated Total Reflectance) accessory. Swelling behavior was analyzed through the water-swelling percentage (WSP), defined as the weight percentage of water uptake by the membranes upon soaking until reaching equilibrium in pure water at 20 °C. WSP was measured by thermogravimetric analysis (TGA), using a TGA Q50 TA Instruments equipment. Samples about 15 mg were first dried in vacuum overnight at 40 °C, and then immersed in water for 12 h. After, TGA tests were performed, under $O_2$ atmosphere, using the next procedure: First, samples were heated under $N_2$ atmosphere, under a flux of 40 ml/min, from RT to 100 °C at 10 °C/min, and then kept during 30 min to completely eliminate the water, obtaining the swelling percentage. Then, TGA analysis was completed by heating up to 800 °C at 10 °C/min, finishing with an isotherm at 800 °C during 10 min under $O_2$ atmosphere. Test were repeated three times to minimize dispersion. To determine the tensile properties of the polymer films, strips of 5 mm in width and 35 mm in length were cut from each polymer film. Tensile tests were carried out on a SHIMADZU EZ Test Compact Table-Top Universal Tester at 20 °C. Mechanical clamps were used and an extension rate of 5 mm/min was applied using a gauge length of 9.44 mm. At least 5 samples were tested for each polymer, and the data was then averaged.

*2.5 – Cellular morphology*

Cellular structural determination of the microcellular films was carried out in a scanning electron microscopy model JEOL JSM-6460LV. Samples were frozen in liquid nitrogen, fractured and gold coated in vacuum to assure the electrical conductivity of the samples. Cellular structural characterization was carried out throughout the determination of the average bubble radius, that was measured using the Image® software from SEM images [23]. The ImageJ® software accounts for the number of bubbles in each image and the average radius. The number average radius $\bar{R}$ is calculated from Equation 1:

$$\bar{R} = \frac{\sum_{i=1}^{N} n_i R_i}{\sum_{i=1}^{N} n_i} \quad (1)$$

, where *N* represents the bubble count. For calculation purposes, at least five different SEM images were analyzed from each material, and the results were averaged. The estimation of the cell density $N_v$ was calculated using the Kumar's approximation, according to Equation 2 [24]:

$$N_V = \left(\frac{n}{A}\right)^{3/2} \quad (2)$$

, where *n* is the number of cells in the image and *A* is the area of the image.

## 3 - Results and discussion

*3.1 – Solid films*

Different solid films were obtained with good surface aspect and homogeneity. Table 1 lists the formulations and the films produced. Five formulations were used, four of them containing the different cross-linking agents (films 2 to 5) and one of them without cross-linker (film 1). , Films were transparent, flexible and also easily manageable. However, flexibility was decreased when

a cross-linking agent of short chain ($M_n$ between 200 and 750) was added to the initial formulation. Each film was cut into three square samples of 35x35 $mm^2$ for foaming experiments. Samples were dried in vacuum at 40 ºC overnight to before measuring their weight. Mass indicated in Table 1 corresponds to the average value from three square samples, which varied slightly from 0.153 to 0.160 g, indicating the homogeneity of the films fabricated.

**Table 1.**

In figure 1 we present a photograph of the solid sample extracted for film 2, together with a SEM micrograph of the film 3, in which the homogeneity of the surface can be seen. The sample surface did not present any cracks or areas with rugosity. Different SEM pictures were captured in different regions of the sample, evidencing a smooth surface.

**Figure 1**.

*3.2 – Microcellular films*

After polymerization process, samples extracted for the films were dried in vacuum at 40 ºC overnight and placed in the high-pressure reactor to carry out the $ScCO_2$ foaming process. In Table 2 we indicate the swelling percentage of $CO_2$ in each film, calculated from Equation 3 by measuring the mass of the samples just after the foaming process:

$$\%\, wt.CO_2 = \frac{m^{foam} - m^{solid}}{m^{solid}} \cdot 100 \qquad (3)$$

, where $m^{foam}$ and $m^{solid}$ indicate the average mass of the samples after and before the foaming process. Values of $m^{solid}$ were taken directly from Table 1, whereas $m^{foam}$ corresponds to the

average mass of the foamed samples just after the foaming process. In addition, in Table 2 the value $m^{final}$ shows the mass of the foamed samples when the desorption process of $CO_2$ is completed. In our case, this value was measured one week after the foaming process, and also after a drying process at 40 ºC in vacuum overnight, to assure that no remaining $CO_2$ and traces of humidity were present in the samples. It is important to remark that the swelling process must be measured not after depressurization, but at the end of the saturation process. These measurements are carried out using a high-pressure magnetic balance placed in the reactor [25]. In our case, measurements of swelling behavior can be only considered as an approximation, which does not take into account the $CO_2$ loss during depressurization.

**Table 2.**

As it is noticed in Table 2, there is a great influence of the molecular mass of the cross-linking agent in the swelling of $CO_2$. Swelling value is reduced from 12.3 % (in samples with no cross-linking agent), to 5.6 % (in samples with **PEGDMA$_{200}$**). Literature reports values of $CO_2$ swelling percentage in methacrylate-based copolymers between 15 and 25 % [26], which shows that reducing the chain length of the cross-linking agent increases the rigidity of the network, thus decreasing the quantity of $CO_2$ absorbed, and consequently, the $CO_2$ swelling percentage. In the case of **PEGDMA$_{20000}$** (sample 6), the swelling percentage is only slightly lower than the swelling percentage of sample 1, with no cross-linking agent added (11.3 and 12.3 %, respectively). It is important to remark that although the addition of the cross-linker implies the presence of polar groups with a $CO_2$ affinity of the ethylene-glycol not negligible (swelling percentage about 5 % at 14 MPa [27]), it is clear that the increased network rigidity associated to the cross-linking effect plays a predominant role in the reduction of the $CO_2$ swelling percentage.

The $CO_2$ desorption process was estimated by measuring the mass of the foamed samples at different times after the foaming process. First, measurements were performed each 5 minutes during two hours. Then, frequency of the measurements was reduced to 30 min during three hours, and after this time, one measurement was carried out each hour during seven hours. After this time, one measurement was carried out each twelve hours up to seven days. Figure 2 shows the $CO_2$ desorption process, in which it can be seen that the equilibrium is reached about three hours after the foaming process, with a remarkable mass decrease observed during the first ten minutes. In this case, no great influence of the molecular mass of the cross-linking agent can be detected.

**Figure 2**.

Figure 3 presents some photographs of the five foamed samples. It is clear that increasing the molecular mass of the cross-linking agent allows for the foaming of the solid sample. Sample with no cross-linking agent (Figure 3a, sample 1f) presents a clear opacity, and also an homogeneous white color. This is a partial indicator of the good foaming behavior of the films, because when a cellular structure is formed, transparency decays due to the diffraction of the light inside the cells, then conferring them a certain degree of opacity. This is valid only for microcellular polymer foams, with cell sizes above 50-100 nm [28]. . On the contrary, the addition of the cross-linking agent of short chain length **PEGDMA$_{750}$** (Figure 3c, sample 3f), makes more difficult the foaming process, showing only isolated regions in which the $CO_2$ sorption is produced, thus conferring low foamability. Finally, sample 5f (Figure 3e), with a cross-linking agent of long chain length, **PEGDMA$_{20000}$**, presents a good foaming behavior, very similar to the behavior observed in sample 1f, in which no cross-linking agent is added.

.

**Figure 3**.

The FTIR spectrum of the **VP-MMA** copolymer is presented in Figure 4. The characteristic absorption bands of **PMMA** are clearly visible, the C=O stretching vibration of ester group appears around 1726 $cm^{-1}$, the doublet bands at 1162 and 1113 $cm^{-1}$ correspond to the C−O stretching vibrations of ester groups [29]. The absorptions around 1421 $cm^{-1}$ characterize the asymmetric bending vibrations of C−$CH_2$ bond. **PVP** represents a strong C=O absorption peak from the amide group of the copolymer at 1656 $cm^{-1}$. A medium strong absorption band of the C−N group appears at 1268 $cm^{-1}$, and C−H stretching vibration frequencies are observed near 2926 $cm^{-1}$. The presence of the cross-linking agent can be clearly detected at the peak variation corresponding to the C-O stretching vibrations of ester groups at 1113 $cm^{-1}$, which is progressively reduced when a cross-linking agent is added. A detailed analysis of the peak variation is depicted in Table 3, which details the peak displacement and also the peak area variation as a function of the molecular mass of the cross-linker. It can be seen that area of the peak is increased with the molecular mass of the cross-linker, indicating that the molecular vibration associated to this region, (C–O stretching vibrations of ester groups), is restricted when the molecular structure of the initial copolymer is cross-linked. For example, in sample 2, with **$PEGDMA_{200}$** in the formulation, the peak disappears completely. It is important to remark that no differences were observed between IR spectra of solid and foamed samples, confirming that during the $ScCO_2$ foaming process the $CO_2$ does not interact or modify chemically the copolymer.

**Figure 4**.

**Table 3.**

The water-swelling percentage (WSP) was obtained directly from the thermogravimetric curves, by simply measuring the weight variation between RT to 100 ºC. It was assumed that the total weight loss during this temperature range was attributed to the water desorption, and no degradation of the copolymer was produced. TGA analysis curves are collected in figure 5. The

influence of the cross-linker in the WSP can be clearly seen: WSP is drastically reduced when cross linker is added (see Figure 5 for detail). This behavior is due to the physical increase of the rigidity of the molecular structure due to the addition of the cross-linker, which makes more difficult the water absorption. Moreover, the cross-linking effect is stronger when the molecular mass is reduced (compare curves of samples 2f and 3f with curves of samples 4f and 5f in Figure 5).

**Figure 5**.

To characterize the thermal stability of the films the extrapolated onset temperature, which denotes the temperature at which the copolymer degradation begins, can be also directly calculated from TGA curves. Table 4 quantifies the WSP percentages and onset temperatures in all the films analyzed.

**Table 4**.

The obtained data show that values of WSP vary between 19 % and 42 %, with a clear influence of the presence of the cross-linker (reported WSP values in similar non-cross-linked films are around 60 % [22], which indicates that the cross-linker reduces greatly the WSP). It can be seen that adding short chain length **PEGDMA**, (film 2f, with **PEGDMA$_{200}$**), decreases the WSP respect to film 1f (without cross-linker) from 42 % to 19 %. This effect is reduced when the molecular weight of **PEGDMA** is increased (see films 4f and 5f, with **PEGDMA$_{8000}$** and **PEDGMA$_{20000}$**, respectively), which shows only slight differences in WSP values respect to film 1f. In this case, the addition of **PEGDMA$_{8000}$** and **PEGDMA$_{20000}$** , increases the WSP due to the hydrophilicity of the cross-linker.

The enhanced rigidity of the films due to the cross-linker addition increases slightly the onset temperature values (between 359 and 383 ºC). Film 2, with **$PEGDMA_{200}$** in the formulation, presented the highest thermal stability, up to 24 ºC higher than film 1, (without cross-linker in the formulation). The effect of the molecular mass of the cross-linker is also evidenced in the onset temperature variation, which decreases from 383 to 361 ºC in films 2 to 5 when increasing the molecular mass of **PEGDMA** from 200 to 20000.

Figure 6 presents the SEM micrographs obtained from samples in the thickness direction. As it can be seen, the addition of **$PEGDMA_{200}$** in the initial copolymer formulation blocks the foaming process, and as a result, solid samples with no cell structure are obtained (Figure 6b). However, increasing the molecular weight of the **PEGDMA** leads to the formation of cellular structures, allowing the foaming of the samples, even when a cross-linked structure is formed in the initial solid sample. Figure 6a presents the cellular structure of sample 1f, with no cross-linker added, in which a bi-modal cellular structure can be appreciated, probably due to the different affinity and diffusivity of the $CO_2$ into the **MMA** and **VP** monomers [25]. This bi-modal structure disappears when the cross-linker is introduced, obtaining a more homogeneous cellular morphology. The inclusion of the cross-linker increases the rigidity of the molecular structure and could limit the bubble expansion equally, thus homogenizing the final bubble radius. Finally, in Figure 6f an overview of the thickness expansion in sample 5f is presented, where it can be seen that final thickness of the foamed films is about 120 μm, indicating an expansion ratio of approximately 20 % respect to the initial thickness of 100 μm. In addition, a very thin solid outer skin with a thickness between approximately 5 and 10 μm can be detected. This type of skin was observed in all the samples.

**Figure 6**.

As shown in figures 6c-e, a correlation between the molecular weight of the cross-linker and the morphological parameters, cell density and cell size, is observed. The quantification of both parameters was carried out using the ImageJ® software, from Equations (1) and (2). Results are summarized in Table 5.

**Table 5**.

Average cell size shows values between 1.02 and 5.34 μm, except sample 2, in which no cellular structure is present, due to the addition of the **PEGDMA$_{200}$**. Increasing the molecular weight of the cross-linker results in higher average cell sizes. Also, the standard deviation value is higher in sample 1f, without cross-linker, presenting a bi-modal cell structure. It is interesting to remark that the addition of the cross-linker reduces the standard deviation value of the average cell radius, homogenizing the cellular structure and also increasing the cell size. This could be due to the good $CO_2$-philicity of the methacrylate groups of the cross-linker, which increases the nucleation sites during saturation process, then reducing the cell size, avoiding coalescence and also increasing the final value of the cell density. Concerning the calculation of cell density $N_c$, the obtained values also increase with $M_n$, lying in the microcellular range $N_c \approx 10^6$. The dependence of $\bar{R}$ and $N_c$ with $M_n$ is represented in Figure 7, in which is evidenced the influence of the molecular weight of the cross-linker in the cellular structure of the foamed films.

**Figure 7**.

Tensile tests were performed in the microcellular films at low velocity (5 mm/min) to evaluate the influence of the cross-linking agent in different mechanical parameters. Young's modulus, stress

and deformation at break point were determined for all the films fabricated. Figure 8 shows the stress-strain ($\sigma$-$\varepsilon$) curves for films 1f to 5f.

**Figure 8**.

As expected, the addition of the cross-linker agent increases the rigidity of the films. Film 1f shows a ductile behavior, with larger deformation at break. Also, film 1f shows a ductile behavior at the end of the test. On the other hand, films 2f to 4f present a typical rigid behavior, with no ductility, and lower values of deformation at break. It is clear that reducing the molecular mass of the cross-linker increases the rigidity of the film, and subsequently, higher young's moduli values are expected. However, film 5f, with **PEGDMA$_{20000}$** in the formulation, does not present a very different behavior from film 1f (with no cross-linker added). The quantification of the mechanical parameters is presented in Table 6. For calculation purposes, the Young's modulus was obtained from the slope of the linear range of the stress-strain curve. In all the cases, the linear region was determined numerically, lying in the deformation range $\varepsilon$ from 0.05 % (in the case of film 2) to 0.1 % (in the case of film 1). The fitting parameter $r^2$ was higher than 0.98 in all the calculations performed. Data presented in Table 6 show, for example, that Young's modulus increases up to one hundred times from film 1f to film 2f (0.01 to 0.98 MPa, respectively). Stress at break point also varies from 1.92 to 8.80 MPa and elongation at break decreases from 578 % to 208 % due to the presence of **PEGDMA$_{200}$**. , The addition of **PEGDMA$_{20000}$** does not affect significantly to the **VP-MMA** copolymer, and films 1f and 5f present similar values of $E$, $\sigma^{break\ point}$ and $\varepsilon^{break\ point}$.

**Table 6**.

Figure 9 evaluates the influence of the molecular mass of the cross-linking agents in the Young's modulus. The experimental values can be fitted using an exponential decay curve, with a value of $r^2$ of 0.9785. Assuming that the absence of cross-linker agent can be equivalent to an addition of a cross-linker of $M_n \rightarrow \infty$, the estimated value of $E$ in the theoretical calculation ($E_0$) is equal to 0.087 MPa, which is in the same order of magnitude than the experimental value found in film 1, with no cross-linker added ($E_{film\ 1f}$ = 0.01 MPa). On the other hand, a cross-linker of very short molecular mass, (thus $M_n \rightarrow 0$), can be assumed as the limit case in which the composition of the film is 100 % cross-linker. In this case, the theoretical value for $E$ is equal to $A$ = 5.081 MPa. To correlate this limit value with experimental data, an additional tensile test was performed in a solid film with composition 100 % of **PEDGMA$_{200}$**, obtaining a Young's modulus value $E$ of 6.74 MPa. Taking into account these approximations, we can conclude that using this simple theoretical correlation, the mechanical properties of cross-linked microcellular films can be estimated as a function of the molecular mass of the cross-linker employed.

**Figure 9**.

## Conclusions

In short, different microcellular polymeric films have been produced using the $ScCO_2$ gas dissolution foaming process. A formulation based on 1-vinyl-2-pyrrolidone and methyl-methacrylate was modified be adding a cross-linker agent, poly(ethylene glycol) dimethacrylate, with different average molecular masses, to evaluate the influence of this parameter in the foaming behavior and in different physical properties, such as thermal stability, water swelling percentage and tensile properties. The IR spectra of the solid films showed a peak variation at 1113 $cm^{-1}$, corresponding to the presence of the cross-linker. It was also found that peak area was directly related to the molecular weight of the cross-linker. The influence of the cross-linker

was evaluated in the thermal stability and water-swelling percentage from thermogravimetric analysis. It was observed that the addition of the cross-linker decreases the water absorption and, at the same time, increases the thermal stability of the films. Both parameters could be controlled by varying the molecular mass of the cross-linker. Next, microcellular films were fabricated using $CO_2$ gas dissolution process. It is well known that cross-linking hinders the $CO_2$ sorption, but in our work, it was observed a good foamability in films with cross-linker of long chain length. In addition, microcellular morphological parameters such as cell density could be tuned as a function of the molecular mass of the cross-linker, increasing as the value of $M_n$ was higher. The films produced presented average cell sizes between 1 and 5 μm and cell density values lying in the microcellular range ($\approx 10^6$ $cm^{-3}$). Finally, the mechanical properties of the films were analyzed by means of low-velocity tensile tests. Microcellular films with cross-linker in their formulation presented an increased rigidity, with higher Young modulus values and lower deformations at break. The influence of the molecular weight of the cross-linker was evaluated and predicted theoretically from the experimental data, correlating the molecular weight of the cross-linker with the Young modulus of the microcellular films.

**Acknowledgments**

## References

[1] J.A.R. Ruiz, M. Pedros, J.M. Tallon, M. Dumon, Micro and nano cellular amorphous polymers (PMMA, PS) in supercritical $CO_2$ assisted by nanostructured $CO_2$-philic block copolymers - One step foaming process, J. Supercrit. Fluids. 58 (2011) 168–176.

[2] S. Costeux, $CO_2$-blown nanocellular foams, J. Appl. Polym. Sci. 131 (2014) 41293(1)-41293(16).

[3] B. Notario, J. Pinto, E. Solorzano, J.A. De Saja, M. Dumon, M.A. Rodríguez-Pérez, Experimental validation of the Knudsen effect in nanocellular polymeric foams, 56 (2015) 57–67.

[4] C. Forest, P. Chaumont, P. Cassagnau, B. Swoboda, P. Sonntag, Polymer nano-foams for insulating applications prepared from $CO_2$ foaming, Prog. Polym. Sci. 41 (2015) 122–145.

[5] J.A. Reglero Ruiz, S. Vallejos, A.M. Sanjuán, F.C. García, M. Múgica, M.A. Rodríguez-Pérez, J.M. García, Microcellular polymeric foams based on 1-vinyl-2-pyrrolidone and butyl-acrylate with tuned thermal conductivity, J. Appl. Polym. Sci. 135 (2017) 45872(1)-45872(7).

[6] B. Notario, J. Pinto, M.A. Rodriguez-Perez, Nanoporous polymeric materials: A new class of materials with enhanced properties, Prog. Mater. Sci. 78–79 (2016) 93–139.

[7] S. Siripurapu, J.A. Coughlan, R.J. Spontak, S.A. Khan, Surface-constrained foaming of polymer thin films with supercritical carbon dioxide, Macromolecules. 37 (2004) 9872–9879.

[8] X.K. Li, G.P. Cao, L.H. Chen, R.H. Zhang, H.L. Liu, Y.H. Shi, Study of the anomalous

sorption behavior of $CO_2$ into poly(methyl methacrylate) films in the vicinity of the critical pressure and temperature using a quartz crystal microbalance (QCM), Langmuir. 29 (2013) 14089–14100.

[9] S. Siripurapu, J.M. DeSimone, S.A. Khan, R.J. Spontak, Low-temperature, surface-mediated foaming of polymer films, Adv. Mater. 16 (2004) 989–994.

[10] S. Siripurapu, J.M. Desimone, R.J. Spontak, S.A. Khan, Generation of nanoporous thin polymer films via foaming with carbon dioxide, Fuel Chem. Div. Prepr. 48 (2003) 262–263.

[11] S. Siripurapu, J.M. DeSimone, S.A. Khan, R.J. Spontak, Controlled foaming of polymer films through restricted surface diffusion and the addition of nanosilica particles or $CO_2$-philic surfactants, Macromolecules. 38 (2005) 2271–2280.

[12] C. Yang, Z. Xing, M. Zhang, Q. Zhao, M. Wang, G. Wu, Supercritical $CO_2$ foaming of radiation crosslinked polypropylene/high-density polyethylene blend: Cell structure and tensile property, Radiat. Phys. Chem. 141 (2017) 276–283.

[13] Z. Jiang, K. Yao, Z. Du, J. Xue, T. Tang, W. Liu, Rigid cross-linked PVC foams with high shear properties: The relationship between mechanical properties and chemical structure of the matrix, Compos. Sci. Technol. 97 (2014) 74–80.

[14] F. Rindfleisch, T.P. DiNoia, M.A. McHugh, Solubility of polymers and copolymers in supercritical $CO_2$, J. Phys. Chem. 100 (1996) 15581-15587.

[15] C. Yang, X. Zhe, M. Zhang, M. Wang, G. Wu, Radiation effects on the foaming of atactic polypropylene with supercritical carbon dioxide, Radiat. Phys. Chem. 131 (2017) 35–40.

[16] D.B. Dias, L.G. de Andrade e Silva, Polyethylene foams cross-linked by electron beam,

Radiat. Phys. Chem. 76 (2007) 1696–1697.

[17] L.O. Salmazo, A. Lopez-Gil, Z.M. Ariff, A.E. Job, M.A. Rodriguez-Perez, Influence of the irradiation dose in the cellular structure of natural rubber foams cross-linked by electron beam irradiation, Ind. Crops Prod. 89 (2016) 339–349.

[18] J.B. Bao, A. Nyantakyi Junior, G.S. Weng, J. Wang, Y.W. Fang, G.H. Hu, Tensile and impact properties of microcellular isotactic polypropylene (PP) foams obtained by supercritical carbon dioxide, J. Supercrit. Fluids. 111 (2016) 63–73.

[19] C. Okolieocha, F. Beckert, M. Herling, J. Breu, R. Mülhaupt, V. Altstädt, Preparation of microcellular low-density PMMA nanocomposite foams: Influence of different fillers on the mechanical, rheological and cell morphological properties, Compos. Sci. Technol. 118 (2015) 108–116.

[20] D. Miller, V. Kumar, Microcellular and nanocellular solid-state polyetherimide (PEI) foams using sub-critical carbon dioxide II. Tensile and impact properties, 52 (2011) 2910–2919.

[21] G. Wang, J. Zhao, L.H. Mark, G. Wang, K. Yu, C. Wang, C.B. Park, G. Zhao, Ultra-tough and super thermal-insulation nanocellular PMMA/TPU, 325 (2017) 632–646.

[22] S. Vallejos, J. Antonio Reglero, F. Clemente García, J. M. García, Direct visual detection and quantification of mercury in fresh fish meat using facilely prepared polymeric sensory labels, (2017) 13710–13716.

[23] J.A.R. Ruiz, J. Marc-Tallon, M. Pedros, M. Dumon, Two-step micro cellular foaming of amorphous polymers in supercritical $CO_2$, J. Supercrit. Fluids. 57 (2011) 87–94.

[24] V. Bernardo, J. Martín-de León, E. Laguna-Gutiérrez, M.A. Rodríguez-Pérez, PMMA-sepiolite nanocomposites as new promising materials for the production of nanocellular

polymers, Euro. Polym. J. 96 (2017) 10-26.

[25] M.M. Hasan, Y.G. Li, G. Li, C.B. Park, Determination of solubilities of $CO_2$ in linear and branched polypropylene using a magnetic suspension balance and a PVT apparatus, J. Chem. Eng. Data 55 (2010) 4885-4895.

[26] K. F. Webb, A. S. Teja, Solubility and diffusion of carbon dioxide in polymers, Fluid Phase Equilib. 158-160 (1999) 1029-1034.

[27] A.C. Galvao, A.Z. Francesconi, Solubility of methane and carbon dioxide in ethylene glycol at pressures up to 14 MPa and temperatures ranging from (303 to 423) K, J. Chem. Thermodyn. 42 (2010) 684-688.

[29] J. Martín-de León, V. Bernardo, M.A. Rodríguez-Pérez, Key production parameters to obtain transparent nanocellular PMMA, Macromol. Mater. Eng. 302 (2017) 1700343(1)-1700343(5).

[29] M.Benadda, M. I. Ferrahi, M. Belbachir, Bull. Synthesis of poly(*N*-vinyl-2-pyrrolidone-co-methyl methacrylate) by maghnite-$H^+$ a Non-toxic Catalyst, Chem. Reac. Eng. Cat. 9 (2014) 201-206.

**List of figures and captions**

**Scheme 1**. Structure of the films

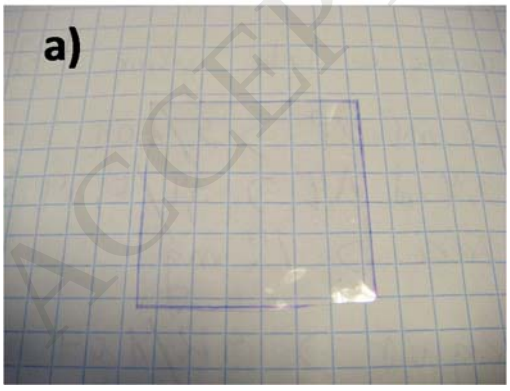


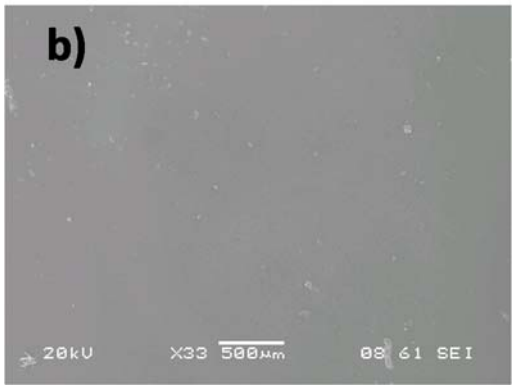

**Figure 1**. Fabricated solid films: a) Photograph of the sample extracted from film 2; b) SEM micrograph of the surface of film 3 (bar scale 500 μm)

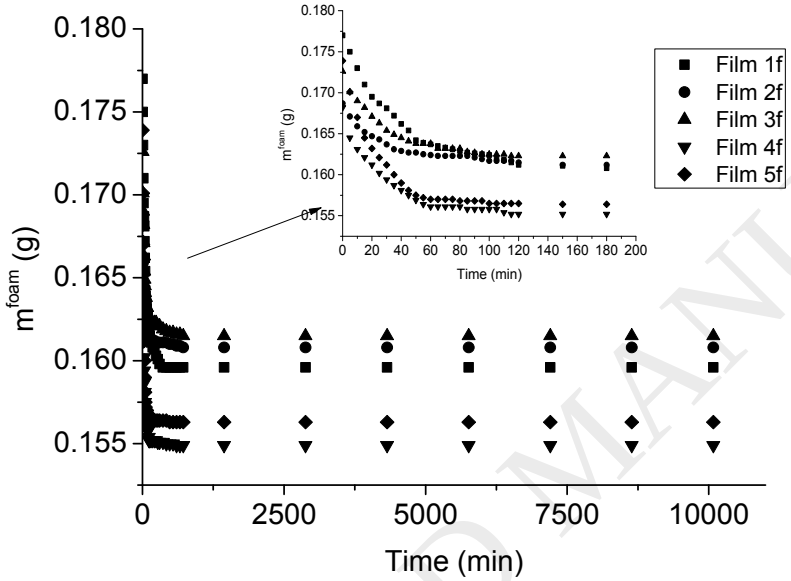


**Figure 2**. Experimental curve showing the desorption of $CO_2$ after the foaming process.

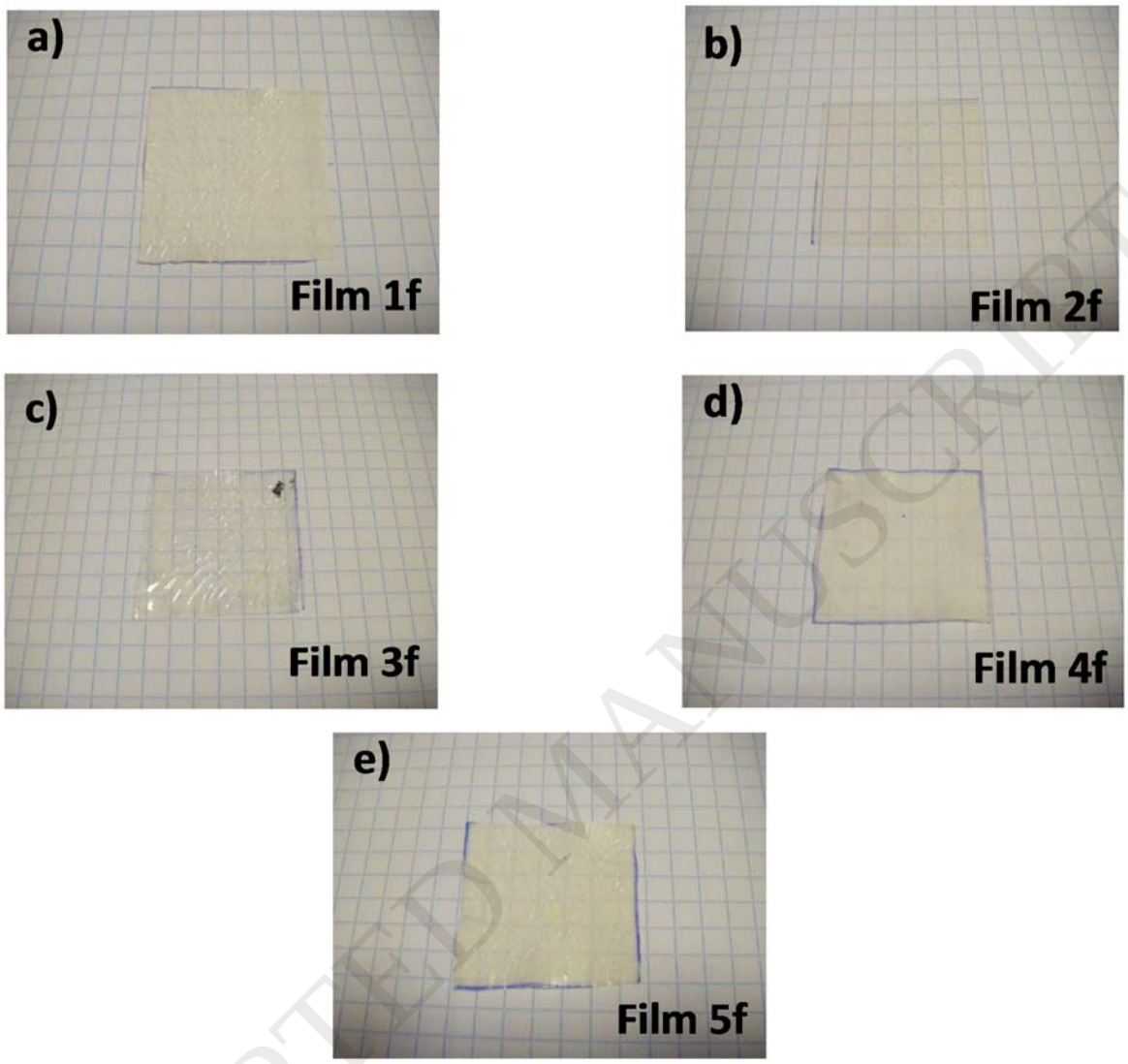


**Figure 3**. Photographs of the foamed samples

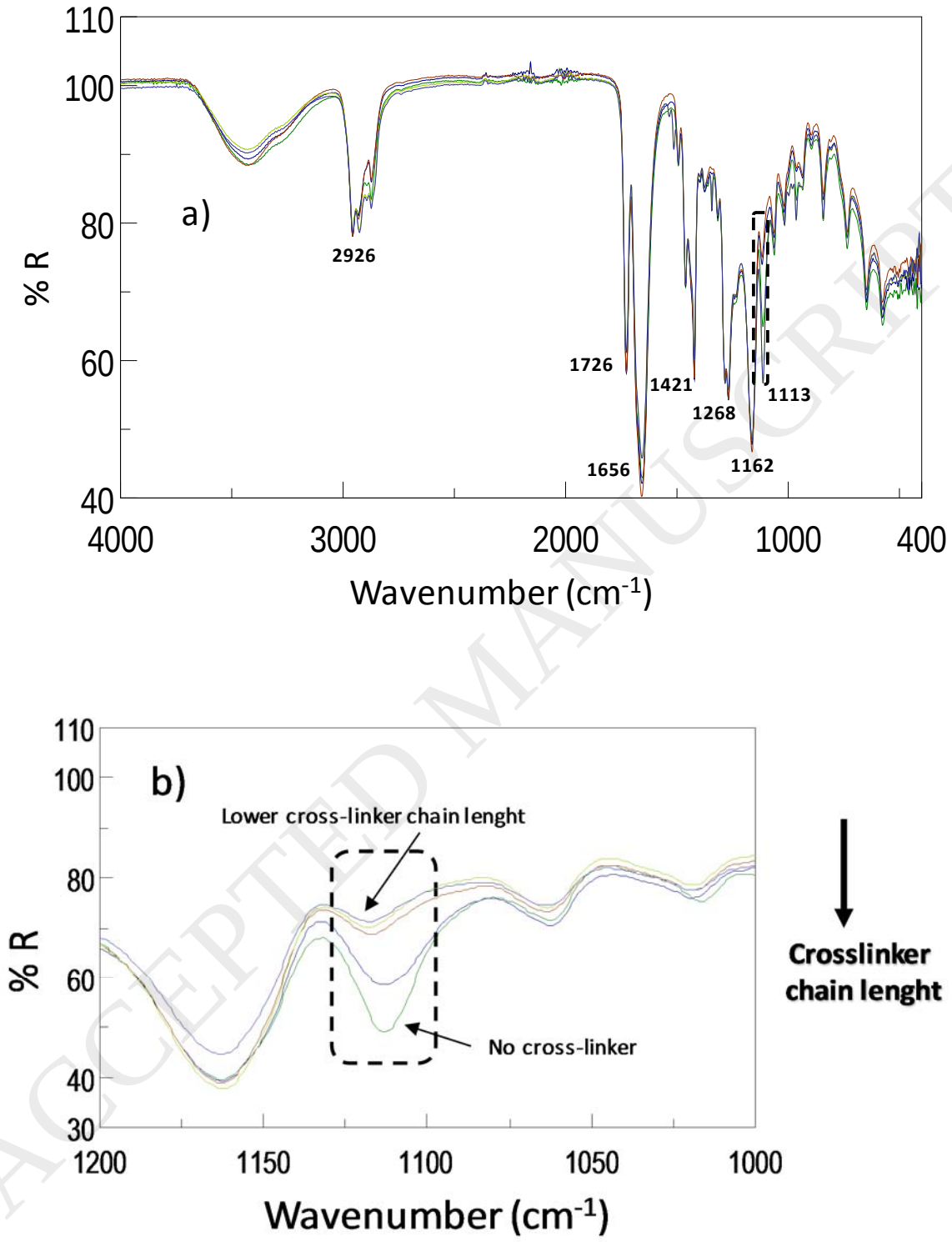


**Figure 4**. IR spectra of the solid materials: a) General spectra ;
b) Detail of the peak variation corresponding to the presence of the cross-linking agent.

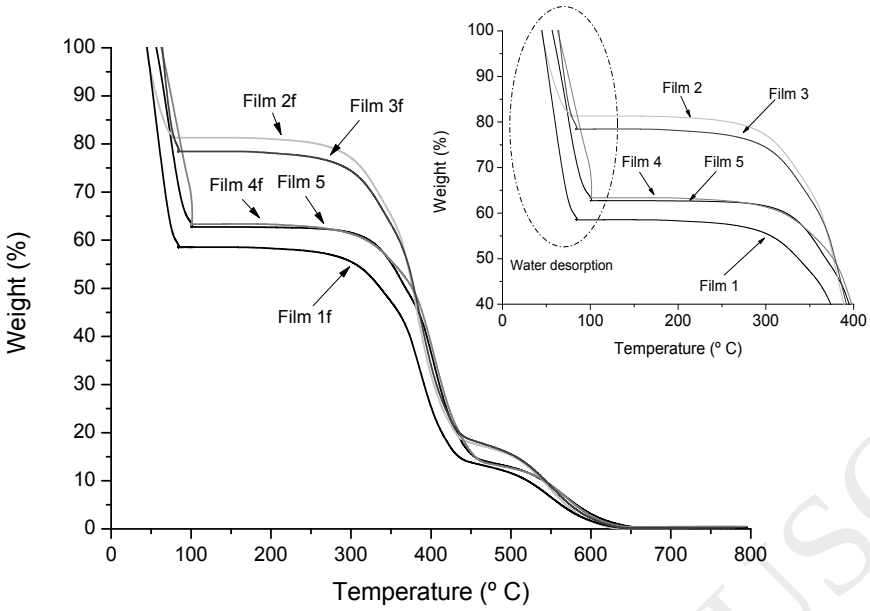


**Figure 5**. Thermogravimetric analysis of the foamed films. Inset: Detail of the curve between RT and 400 ºC.

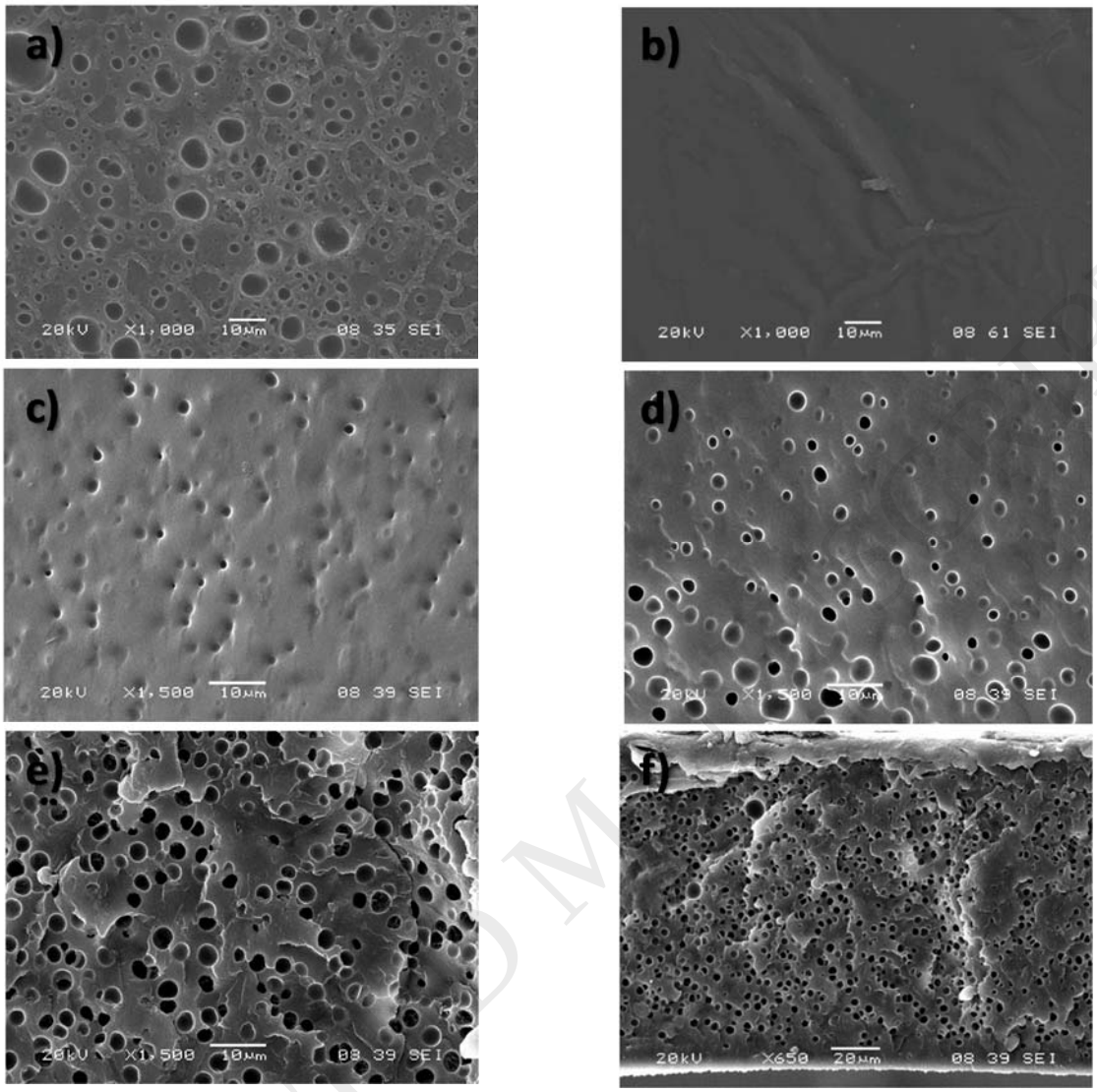


**Figure 6**. SEM micrographs of the foamed samples: a) Sample 1f ; b) Sample 2f ; c) Sample 3f d) Sample 4f ; e) Sample 5f ; f) Overview of thickness expansion in sample 5f.

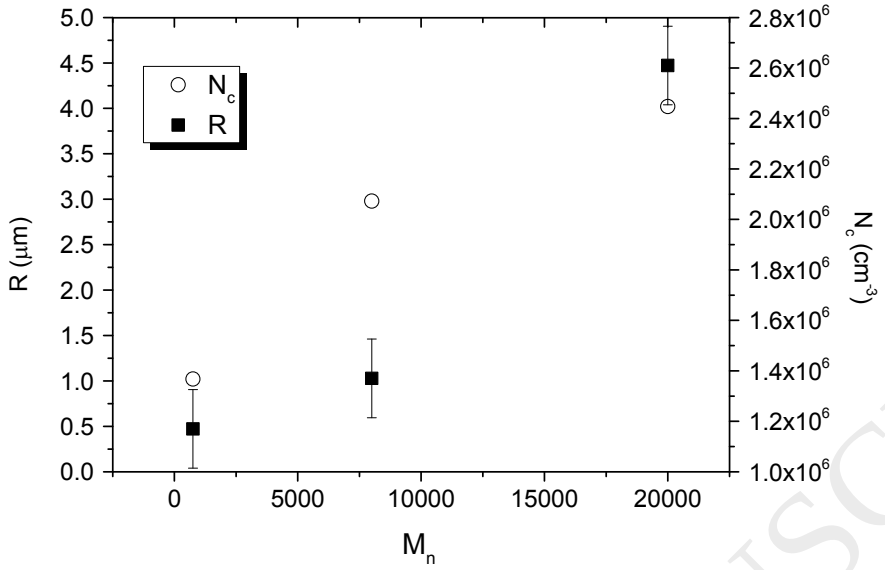


**Figure 7**. Dependence of average cell size and cell density with the molecular mass of the cross-linker.

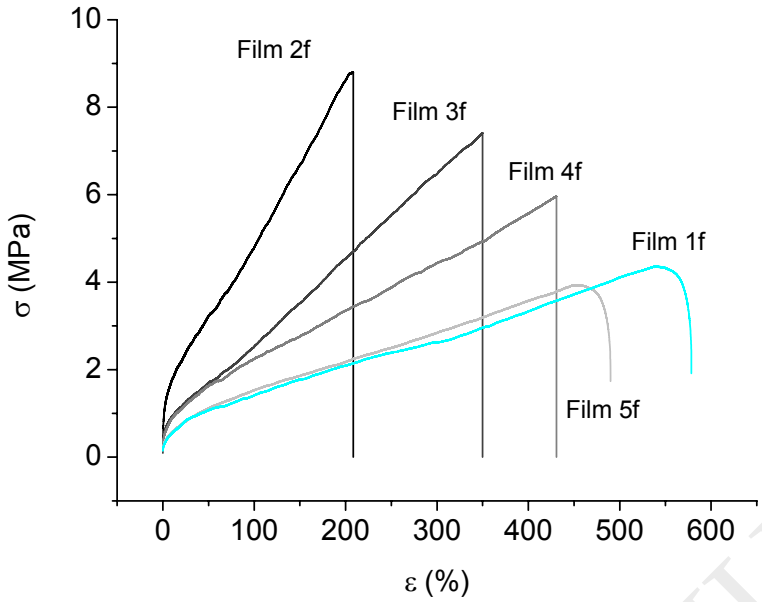


**Figure 8**. Stress-strain curves obtained from tensile tests at 5 mm/min.

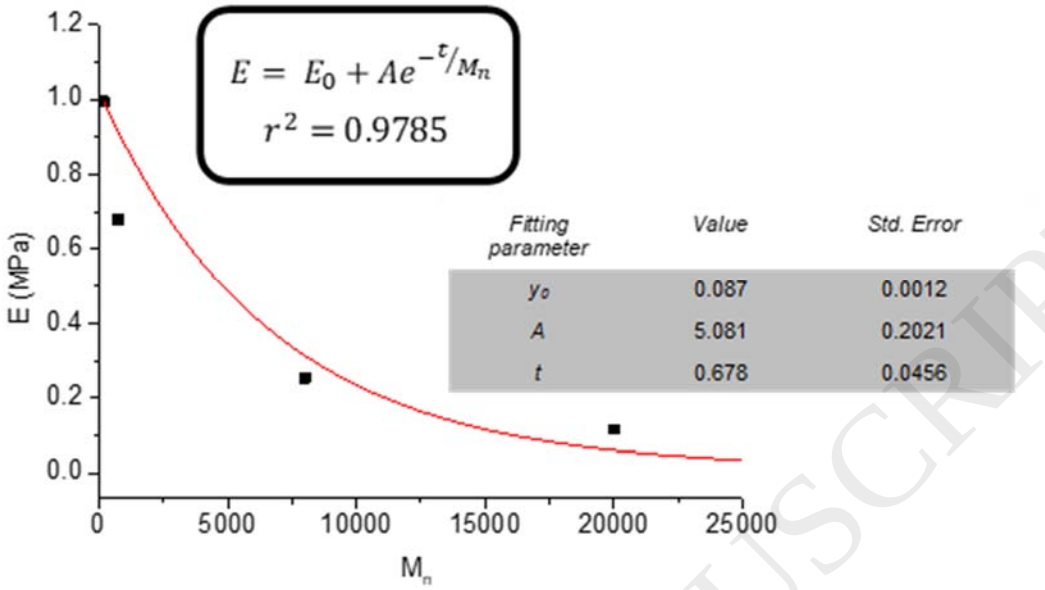


**Figure 9**. Young's modulus as function of mass number average of the cross-linker.

## Tables

**Table 1.** Formulations employed in this work and films fabricated

| *Film number* | *Formulation (VP/MMA/PEGDMA)* | *Cross-linker* | *Mass[solid a)] (g)* |
|---|---|---|---|
| 1 | 50/50/0 | Not added | 0.1577 |
| 2 | 49.9925/49.9925/0.015 | $PEGDMA_{200}$ | 0.1598 |
| 3 | 49.9925/49.9925/0.015 | $PEGDMA_{750}$ | 0.1602 |
| 4 | 49.9925/49.9925/0.015 | $PEGDMA_{8000}$ | 0.1534 |
| 5 | 49.9925/49.9925/0.015 | $PEGDMA_{20000}$ | 0.1563 |

a) Indicates the average mass of the three cut samples of 35 x 35 $mm^2$

**Table 2.** Physical characteristics of the foamed films

| *Film number* | *Mass[foam a)] (g)* | *$CO_2$ uptake [b)] (% wt.)* | *Mass[final c)] (g)* |
|---|---|---|---|
| 1f | 0.1770 | 12.3 | 0.1596 |
| 2f | 0.1687 | 5.6 | 0.1608 |
| 3f | 0.1726 | 7.8 | 0.1615 |
| 4f | 0.1682 | 9.7 | 0.1549 |
| 5f | 0.1739 | 11.3 | 0.1593 |

a) Indicates the average mass of the three samples measured just after the foaming experiment

b) Indicates the average percentage of mass uptake of $CO_2$ just after the foaming experiment

c) Indicates the average mass of the three samples measured one week after the foaming experiment

**Table 3.** Characteristics of the IR absorption peak around 1113 $cm^{-1}$ in solid films

| *Film number* | *Cross-linker* | *Wavenumber ($cm^{-1}$)* | *Peak area* |
|---|---|---|---|
| 1 | Not added | 1112.9 | 271.23 |
| 2 | $PEGDMA_{200}$ | 1119.0 | 137.21 |
| 3 | $PEGDMA_{750}$ | 1117.2 | 142.26 |
| 4 | $PEGDMA_{8000}$ | 1115.5 | 159.97 |
| 5 | $PEGDMA_{20000}$ | 1113.1 | 251.27 |

**Table 4.** Water swelling percentage (WSP) and onset temperature of the foamed films obtained from TGA measurements (all tests performed in $N_2$ atmosphere)

| *Film number* | *WSP (%)* | *Onset temperature (ºC)* |
|---|---|---|
| 1f | 42 | 359 |
| 2f | 19 | 383 |
| 3f | 22 | 378 |
| 4f | 37 | 371 |
| 5f | 38 | 361 |

**Table 5.** Morphological parameters of the foamed films

| *Film number* | $\bar{R}$ *(μm)* | *Desv. Std* | *n* | *A* *(μm²)* | $N_c$ *(cm⁻³)* |
|---|---|---|---|---|---|
| 1f | 5.34 | 0.980 | 256 | 11408 | $2.24 \times 10^6$ |
| 2f | N/A | N/A | N/A | 11408 | N/A |
| 3f | 1.02 | 0.013 | 134 | 11408 | $1.17 \times 10^6$ |
| 4f | 2.98 | 0.230 | 157 | 11408 | $1.37 \times 10^6$ |
| 5f | 4.02 | 0.091 | 298 | 11408 | $2.61 \times 10^6$ |

$\bar{R}$ indicates the average cell radius ; *n* indicates the bubble count number ; *A* indicates the micrograph area ; $N_c$ indicates the cell density

**Table 6.** Mechanical parameters of the foamed films obtained from tensile tests at 5 mm/min

| *Film number* | *E* *(MPa)* | $\sigma^{break\ point}$ *(MPa)* | $\varepsilon^{break\ point}$ *(%)* |
|---|---|---|---|
| 1f | 0.01 | 1.92 | 578 |
| 2f | 0.98 | 8.80 | 208 |
| 3f | 0.67 | 7.41 | 350 |
| 4f | 0.25 | 5.96 | 431 |
| 5f | 0.11 | 1.73 | 489 |